

# Final Report for YSU Center of Transportation and Materials Engineering (YSU CTME)

**Project Title:**

Hydrothermal Synthesis and Shape-  
Reactivity Correlation Study of  
Automotive Three-Way Nanocatalysts

**Prepared by:**

Ruigang Wang (PI)  
Department of Chemistry  
Youngstown State University

## DISCLAIMER

*The content of this report reflect the views of the authors, who are Responsible for the facts and the accuracy of the information presented herein. This document is disseminated under the sponsorship of the Department of Transportation University Transportation Centers Program, in the interest of information exchange. The U.S. Government assumes no liability for the Contents or use thereof.*

**2/12/2014**

**Summary:** In this project, we have shown that the hydrothermal method can be used to tune the shape/size of CeO<sub>2</sub> nanocrystals. CeO<sub>2</sub> nanorods and nanocubes have been successfully prepared at low and high hydrothermal reaction temperature, respectively. The chemisorption analysis and CO oxidation test evidenced that a high oxygen vacancy concentration in CeO<sub>2</sub> nanorods leads to a lower temperature reducibility and superior catalytic activity, compared to CeO<sub>2</sub> nanocubes. Out of this project, three refereed and two proceeding papers were published, along with several oral presentations made by PI and students.

## 1. Major Accomplishments

Phase purity of the samples was quantified using Powder X-ray diffraction. As shown in Fig. 1, all diffraction peaks were indexed to the cubic fluorite structure (JCPDS card number 34-0394) confirming that the two samples were pure  $\text{CeO}_2$ . The diffraction peaks corresponding to nanocubes are slightly shifted to higher angles while those corresponding to nanorods are slightly shifted to lower angles (this observation is highlighted by the green dotted lines in Fig. 1 below). This implies that the crystal planes of the nanocubes have shorter d-spacing and a smaller lattice constant while those of nanorods have a bigger d-spacing and a larger lattice constant. The calculated particle size of nanorods and nanocubes are 8.2 nm and 20.3 nm, respectively. The (hkl) miller indices and d-spacing data were used to compute lattice constant information. Calculations revealed that nanorods and nanocubes had lattice constants of 5.429 Å and 5.413 Å respectively, implying that lattice constants decrease with increasing particle size. The lattice constant difference could also be due to the lattice strain caused by the lattice oxygen vacancy in ceria nanorods.

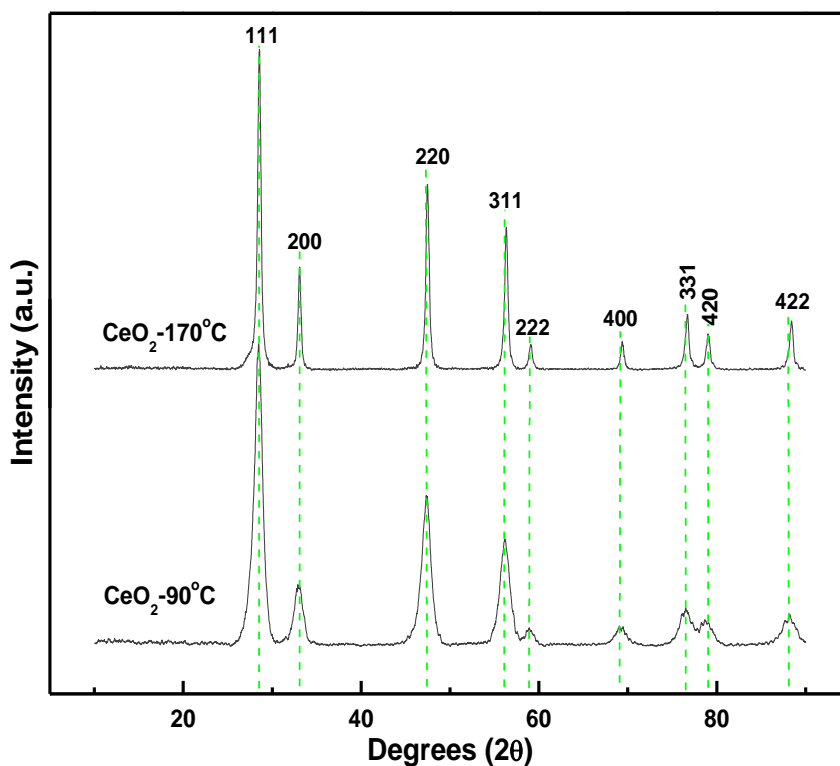


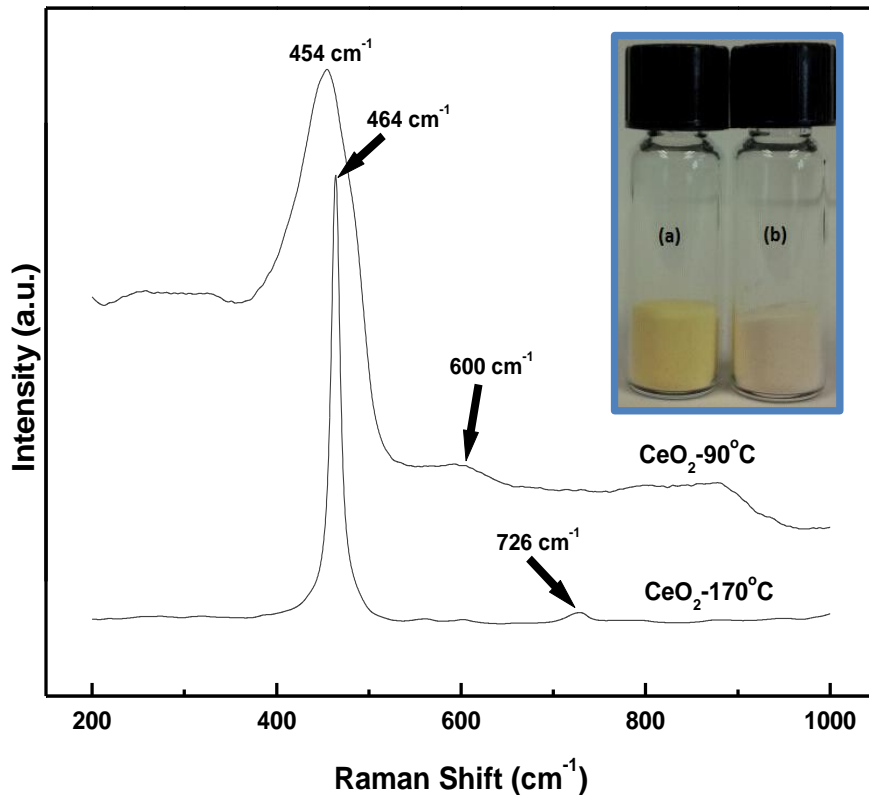
**Figure 1.** Powder XRD patterns of  $\text{CeO}_2$  nanorods and nanocubes prepared by the hydrothermal reactions at different temperature.

BET surface area analyses revealed that nanorods have higher surface area as compared to nanocubes (see Table 1 below). We attribute this to the fact that nanorods are of a smaller size. Table 1 below is a summary of the particle size, lattice constant, and BET surface area data for  $\text{CeO}_2$  nanorods and nanocubes.

**Table 1.** Particle size and lattice constant data for pure ceria samples

Sample Identity	Particle Size (nm)	Lattice Constant ( $\text{\AA}$ )	BET Surface Area
Ceria nanorods	8.246	5.429	78.73
Ceria nanocubes	20.344	5.413	37.63

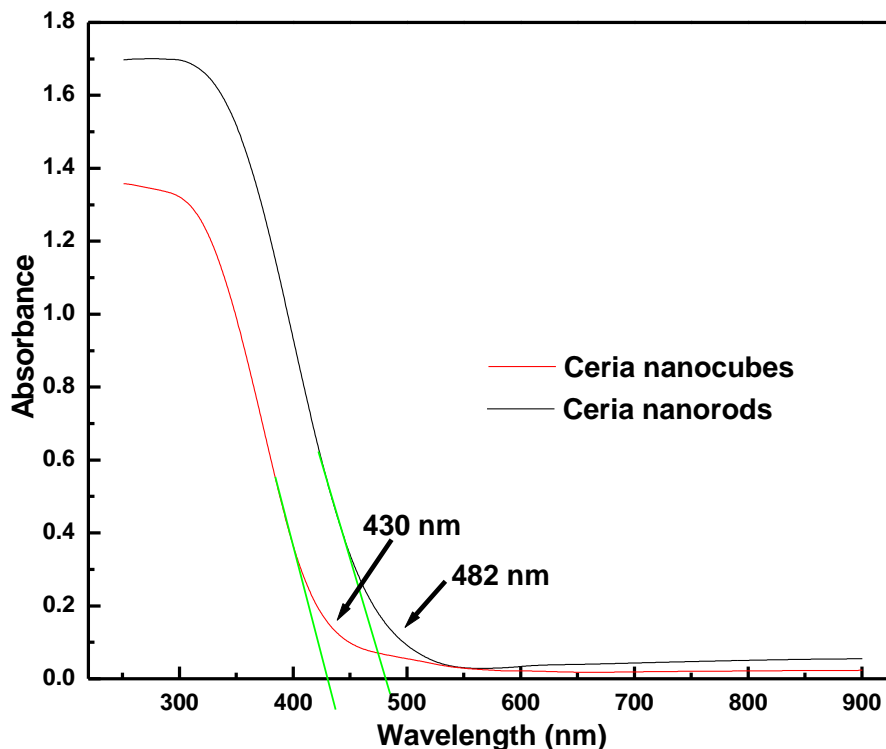
Fig. 2 shows the Raman spectra and the color of the  $\text{CeO}_2$  nanorods and nanocubes samples. In both spectra, first order scattering peaks appear at  $454 \text{ cm}^{-1}$  and  $464 \text{ cm}^{-1}$  for nanorods and nanocubes respectively while second order scattering peaks appear at  $600 \text{ cm}^{-1}$  and  $726 \text{ cm}^{-1}$  for nanorods and nanocubes respectively. The first order peaks are evidence of symmetric vibrations of the F2g modes of  $\text{CeO}_2$  while the second order peaks can be ascribed to extrinsic oxygen vacancies present in the samples. Upon closer inspection, it is evident that the second order peaks of these samples feature different intensities. These peak disparities arise from differences in the oxygen vacancy concentrations per unit cell volume of the material. Specifically, the greater intensity of the nanorod's second order peak at  $600 \text{ cm}^{-1}$  compared to the nanocube's second order peak at  $726 \text{ cm}^{-1}$  reveals that nanorods have higher oxygen vacancies compared to nanocubes.



**Figure 2.** Raman spectroscopy data. Inset picture shows color of (a) ceria nanorods and (b) ceria nanocubes.

Interestingly as shown in the inset picture on Fig. 2, the two nanopowders assume different colors despite their identical chemical composition. Our hypothesis is that the yellow color in ceria nanorods is as a result of high oxygen vacancy concentration and a rough surface morphology (as will be shown in the TEM images).

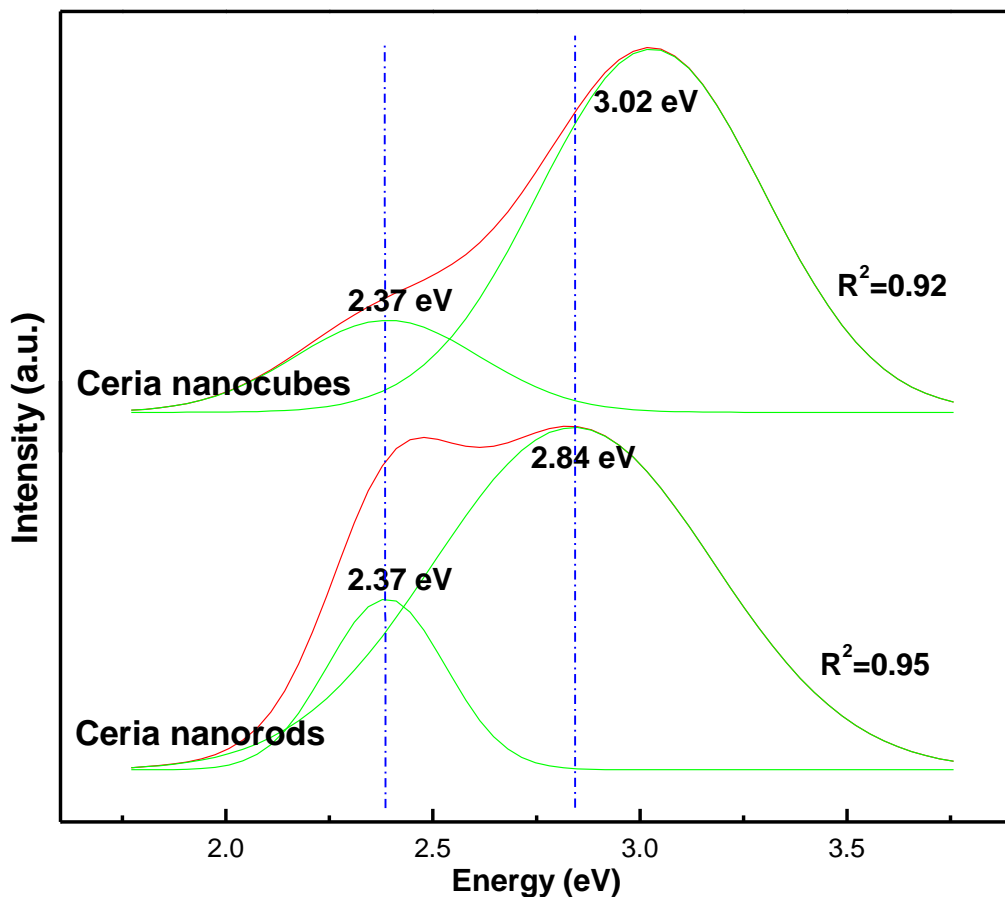
Fig. 3 shows the UV-VIS absorption spectra for the nanopowders. The absorption spectra have the same general shape with a slight difference in magnitude. From the data, it is clear that the onset of the absorption band for nanorods occurs at around 482 nm while that of nanocubes occurs at around 430 nm. These absorption edges correspond to band gap energies of 2.78 eV and 3.11 eV for nanorods and nanocubes respectively. We therefore hereby state categorically that the band gap of cerium oxide nanoparticles could be engineered through varying their particle size and morphology. The disparity in the band gap size of the two samples stems from the fact that nanorods have a higher oxygen vacancy density and a higher content of  $Ce^{3+}$  ions compared to the nanocubes.



**Figure 3.** UV-Vis data indicating the onset of absorption spectra in ceria nanopowders.

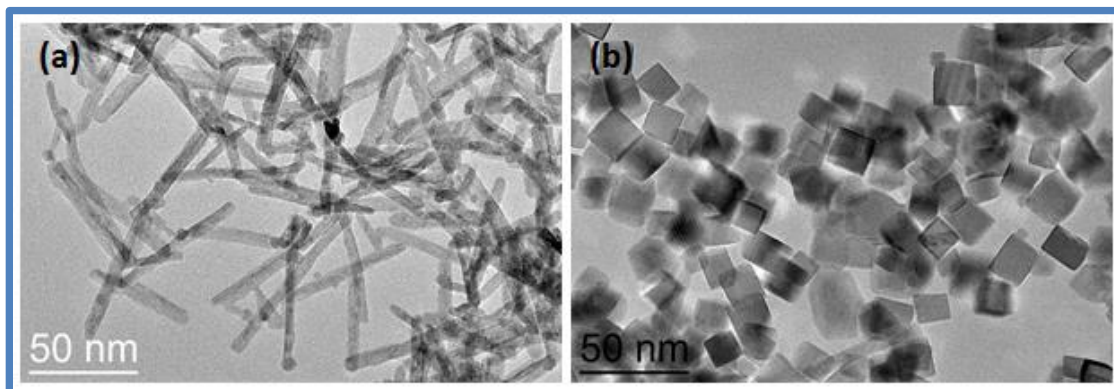
Fig. 4 presents Photoluminescence spectra for the nanopowders. The spectra are in very good agreement with UV-Vis and Raman spec data that have been presented above. Inspection of the spectra shows that the bandgap of nanorods is 2.84 eV while that of nanocubes is 3.02 eV. As was mentioned earlier, these energies correspond to the  $O_{2p}-Ce_{4f}$  transitions in ceria. In addition to the band gap information, the figure also gives other information regarding the density of oxygen vacancies. Emissions that occur at around 2.37 eV in both nanorods and nanocubes can be associated with the intermediate energy levels that occur within the band gap of the nanoparticles. These intermediate levels are believed to consist of 2p states near the valence band and cerium 5d levels below the conduction band. In these intermediate levels, excitation processes occur when electrons are promoted from the oxygen 2p states to cerium 5d levels through the absorption of photons while emission processes occur when electrons localized in the cerium 5d levels decay into empty oxygen 2p states. The relative intensities and areas of these peaks compared to those that occur at higher energies and the total area of the spectra may be used to relay special information regarding to the extent of oxygen vacancies in

the materials. Based on the intensities and areas of the low energy (2.37 eV) peaks, it can therefore be concluded that ceria nanorods have a higher density of oxygen vacancies as compare to the nanocubes.



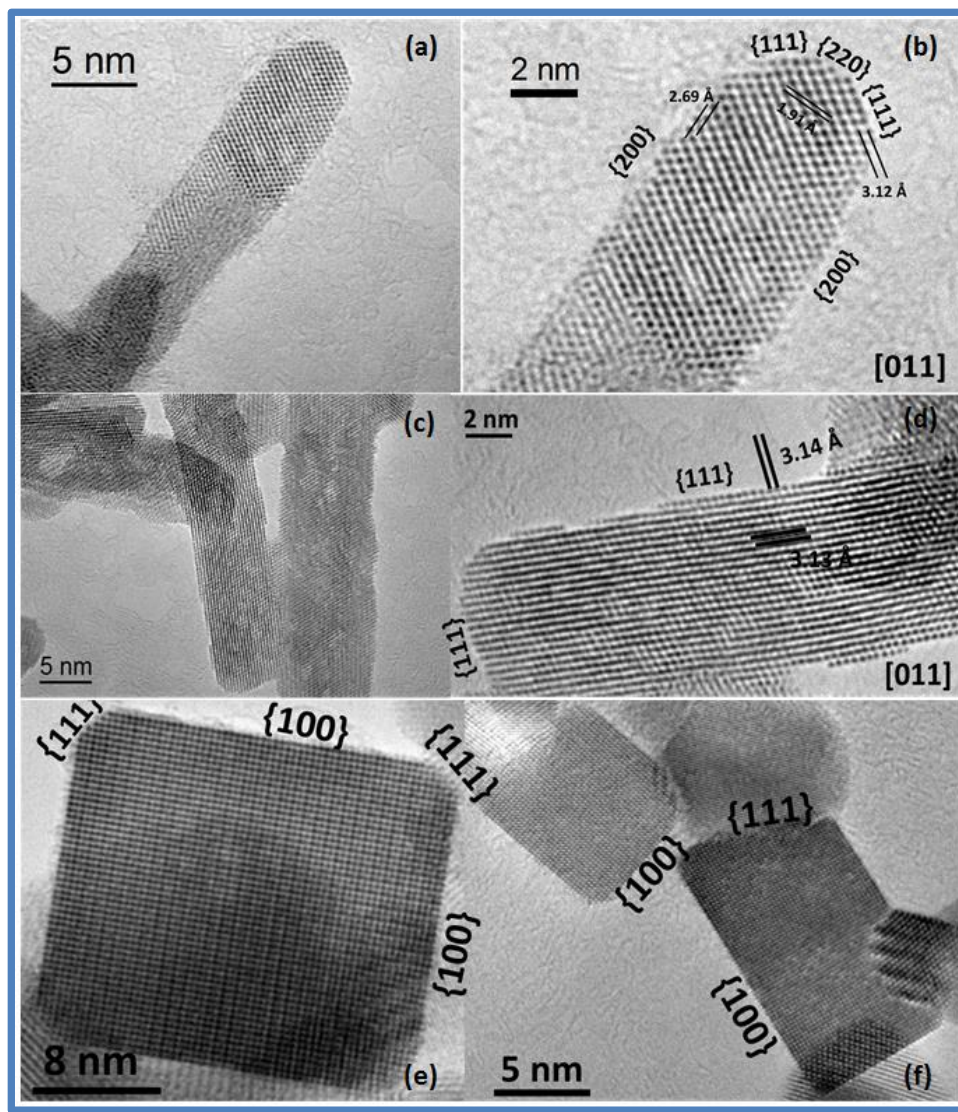
**Figure 4.** Gaussian fitting of Photoluminescence spectra for ceria nanorods and nanocubes.

Figure 5 is a compilation of low magnification TEM images of the samples. From the data, it is easy to tell that different synthesis temperatures lead to different morphologies and size. Nanoparticles in both samples are well dispersed with negligible agglomeration.



**Figure 5.** Low magnification TEM images of (a) ceria nanorods and (b) ceria nanocubes.

Close inspection of Fig. 6 shows that nanocubes are highly isotropic with each having a length of roughly 20 nm. Nanorods on the other side are comprised of multiple tiny crystals and each has a length of roughly 50 nm and a width of roughly 5 nm. It is believed that nanorods grow anisotropically since they have rough surfaces and are composed of multiple tiny crystals. Also, it is easy to note that crystal size and dispersion from TEM data are consistent with XRD and BET surface area analyses. Theoretical studies have shown that oxygen vacancy formation energies in different CeO<sub>2</sub> surfaces follow the  $\{110\} < \{100\} < \{111\}$  sequence. In order to determine whether our samples were consistent with this theory, HRTEM analyses were performed as shown on Fig. 6 after which H<sub>2</sub>-TPR and CO conversion studies were then performed on the samples in order to correlate their low temperature reducibility and oxygen storage capacity to their exposed crystallographic facets. Our findings reveals that nanorods are  $\{220\}$ ,  $\{200\}$ , and  $\{111\}$  terminated while nanocubes were  $\{100\}$  and  $\{111\}$  terminated. These results are consistent with theory as  $\{200\}$  and  $\{220\}$  facets belong to the same family as  $\{100\}$  and  $\{110\}$  facets respectively.



**Figure 6.** HRTEM images for ceria nanorods (a-d) and nanocubes (e-f).

Fig. 7 shows the H<sub>2</sub>-TPR profiles for the samples. As can be observed from the data, ceria nanorods are characterized by three distinct surface and subsurface reduction bands that occur at 54.5°C, 410°C and 480°C while the peak that appears at 773°C represents bulk or lattice oxygen reduction. Ceria nanocubes on the other hand are characterized by two overlapped low intensity surface reduction bands at 382°C and 504°C and a higher temperature bulk reduction peak at 784.75°C. Based on the intensities of the surface reduction peaks, it is easy to note that ceria nanorods have higher low temperature reducibility compared to nanocubes. These observations are in agreements with HRTEM images as nanorods are seen to majorly contain {110} and {100} surfaces that are believed to release oxygen at lower reaction temperatures as compared to nanocubes that are majorly dominated by {100} surfaces. Ceria nanorods show higher low temperature reducibility as compared to nanocubes. In fact, it is even noted that nanorods showed a small reduction band at 55.5°C while nanocubes did not show any noticeable signs of reduction between room temperature and 350°C. We therefore concluded that reduction in ceria nanorods is surface dominated and requires a comparatively low amount of thermal energy to occur while the reduction of ceria nanocubes is bulk dominated and requires a high amount of thermal energy to take place. We attributed these unique observations to the fact that ceria nanorods have a narrower band gap compared to nanocubes and therefore encounter less potential energy barrier in achieving Ce<sup>4+</sup>/Ce<sup>3+</sup> charge transfer during reduction processes. As mentioned above, these observations are in good agreement with theory.

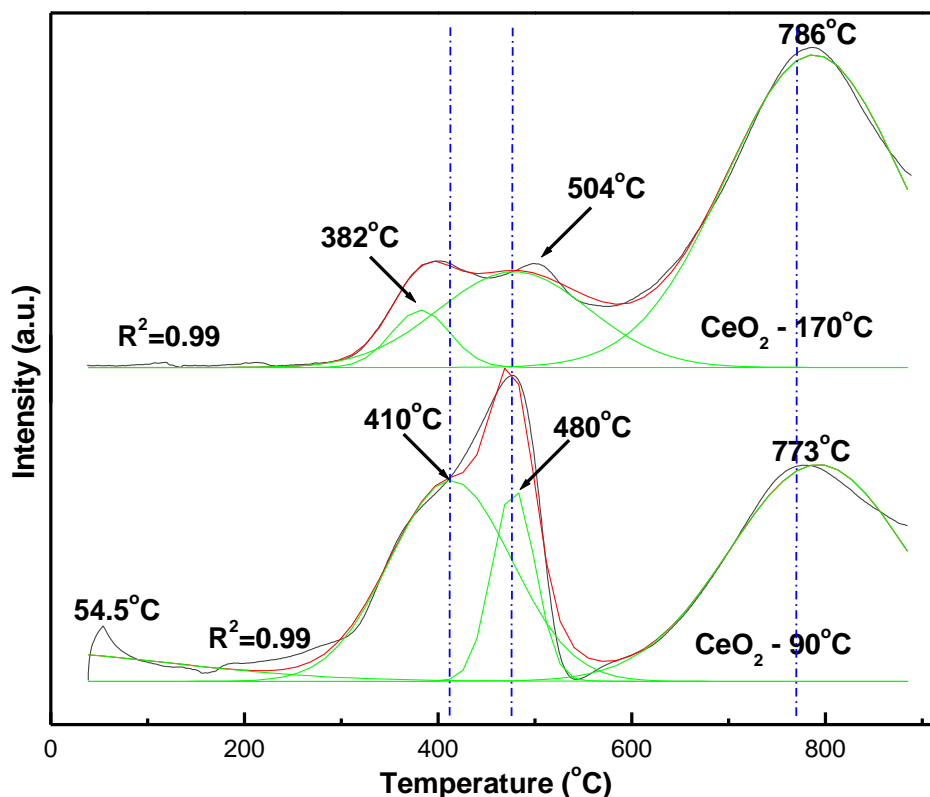


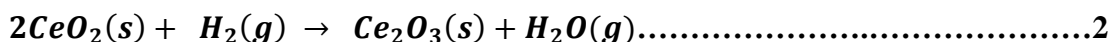
**Figure 7: Gaussian plots of TPR data**

Hydrogen consumption and oxygen storage capacity estimations were also carried out by using the above plotted TPR data. In order to carry out accurate computations, peak area

calibrations were first done by reducing known masses of Cu<sub>2</sub>O to Cu metal after which the corresponding peak areas were converted to moles of hydrogen that had been consumed in the reaction according to the chemical equation below:



Similar computations were then performed in calculating the moles of hydrogen that were consumed per each mole of ceria nanoparticles. It is believed that ceria (IV) oxide reduces to ceria (III) oxide according to the equation below where theoretically speaking, one mole of cerium (IV) oxide combines with 0.5 moles of H<sub>2</sub> to generate 0.5 moles of cerium (III) oxide and 0.5 moles of H<sub>2</sub>O. This implies that one mole of cerium (IV) oxide should theoretically donate 0.5 moles of O atoms and should consume 0.5 moles of H<sub>2</sub> assuming 100% conversion of cerium (IV) oxide to cerium (III) oxide. However, our calculations revealed that it is not possible to reduce these materials to a perfect Ce<sub>2</sub>O<sub>3</sub> structure. In fact, nanorods offered less than 50% of the theoretically predetermined oxygen storage capacity while nanocubes offered slightly more than 50% of the theoretical figure.



Our calculations are summarized in the table below, from which it is clear that ceria nanocubes offer a higher hydrogen consumption as compared to nanorods although nanorods offer a higher low temperature reducibility as was discussed earlier on. These observations are a manifestation of the effect of oxygen vacancy concentration in the lattice structure of ceria. Comparison of Table 3 and Figs. 4 & 7 shows clearly that a higher concentration of oxygen vacancies in ceria nanorods leads to lower hydrogen consumption and lower oxygen storage capacity while a lower concentration of the same in ceria nanocubes leads to higher hydrogen consumption and higher oxygen storage capacity compared. Consequently, this difference in the concentration of oxygen vacancies in the nanoshape leads to an enhanced low temperature reducibility in nanocubes and a poor low temperature reducibility in nanorods.

**Table 2.** A summary of hydrogen consumption and oxygen storage capacity data.

Sample identity	Surface reduction peak area	Bulk reduction peak area	Surface hydrogen consumption (H <sub>2</sub> Moles/CeO <sub>2</sub> moles)	Bulk hydrogen consumption (H <sub>2</sub> Moles/mole of CeO <sub>2</sub> )	Total H <sub>2</sub> consumption (H <sub>2</sub> Moles/mole of CeO <sub>2</sub> )	Corresponding O storage capacity (O moles/mole of CeO <sub>2</sub> )
Nanorods	2.1833	1.93118	0.1	0.09	0.19	0.19
Nanocubes	2.5206	4.80839	0.11	0.22	0.33	0.33

Fig. 8 is a plot of CO oxidation profiles. It is clear from the data that nanorods have the capacity to neutralize CO at relatively lower temperatures as compared to nanocubes. For

example, comparison of the profiles indicates that the oxidation of CO over ceria nanorods begins to occur at just above 75°C while nanocubes begin to neutralize CO at temperatures well above 175°C. In addition, the light off temperatures for nanorods and nanocubes are 242°C and 270°C respectively. Ultimately, nanorods show complete CO neutralization at around 317°C while nanocubes begin to show 100% CO conversion at temperatures above 350°C. These catalytic differences can only be attributed to the crystallographic and morphological disparities between ceria nanorods and nanocubes. As was mentioned above, these catalytic performance disparities stem from the fact that the two samples have different crystallographic and electronic properties.

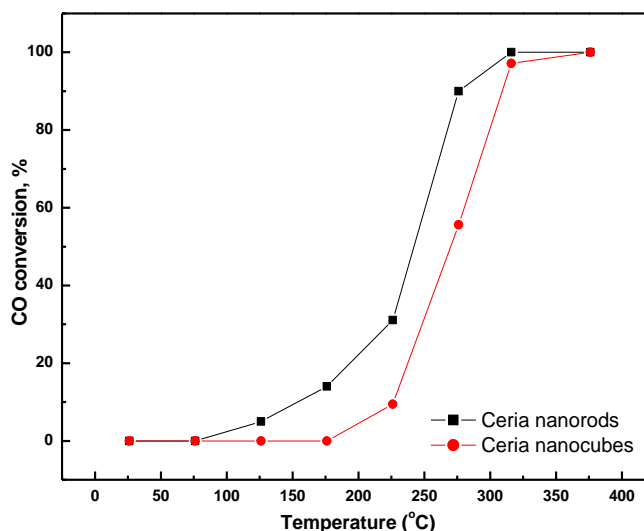


**Figure 8.** CO conversion as a function of temperature.

## 2. Student Researchers Involved in This Grant:

Name (s)	Affiliation	Job Description
Samuel Mutinda (PhD graduate)	YSU, Chemistry	Catalytic activity and TEM characterization
Varun Sama (MS graduate)	YSU, Chemistry	Surface analysis of materials and heterogeneous catalysts
Aron Korir (Undergraduate)	YSU, Chemistry and Forensic Science	solution based oxide nanomaterials synthesis and characterization
Randi Dangerfield (Undergraduate)	YSU, Chemistry	solution based oxide nanomaterials synthesis and characterization
Zach Brown (Undergraduate)	YSU, Chemistry	solution based oxide nanomaterials synthesis and characterization

## 3. Listing of Journal Publications and Conference Presentation Resulting from This Grant

- R. Wang, R. Dangerfield, Seed-mediated hydrothermal synthesis of shape-controlled CeO<sub>2</sub> nanocrystals, *RSC Advances*, 4(7): 3615-3620 (2014)
- R. Wang, S. Mutinda, Minghao Fang, One-pot synthesis and high temperature thermal stability in Ce<sub>x</sub>Zr<sub>1-x</sub>O<sub>2</sub> nanocrystals, *RSC Advances*, 3(42): 19508-19514 (2013)
- R. Dangerfield, D. Li, R. Wang, Low-temperature CO conversion on 1wt%Pt/CeO<sub>2</sub> nanocrystals, *Microsc Microanal* 19(Suppl 2): 1700-1701 (2013)
- R. Wang, V. Sama, D. Li, S.I. Mutinda, Hydrothermal synthesis of rare-earth oxide nanocatalysts for automotive exhaust clean-up, *Advanced Materials Research*, 512-515: 1624-1629 (2012)
- R. Wang, S.I. Mutinda, D. Li, Size/shape-controlled synthesis and low-temperature reactivity of ceria, *Microsc Microanal* 18(Suppl 2): 1394-1395 (2012)
- R. Wang, M. Fang, Improved low-temperature reducibility in ceria zirconia nanoparticles by redox treatment, *J. Mater. Chem.*, 22: 1770-1773 (2012)
- R. Dangerfield, D. Li, R. Wang, Low-Temperature CO Conversion on 1wt%Pt/CeO<sub>2</sub> Nanocubes, *Microscopy & Microanalysis 2013*, Indianapolis, Indiana USA, August 4-8, 2013
- R. Dangerfield, R. Wang, Shape/Size-Reactivity Correlation Study in CeO<sub>2</sub> Nanocrystals, **23<sup>rd</sup> North America Catalysis Society Meeting**, Louisville, Kentucky USA, June 2-7, 2013
- (*Best Undergraduate Student Poster Award*) R. Dangerfield, R. Wang, Hydrothermal Synthesis and Reactivity Characterization of Ceria Nanoparticles, *American Chemical Society –The Penn Ohio Border Section Award Banquet*, Westminster College, New Wilmington, PA USA, April 19, 2013
- V. Sama, R. Wang, Synthesis and Characterization of CeO<sub>2</sub>-TiO<sub>2</sub> Nanotubes, *YSU Quest 2013*, Youngstown, Ohio USA, April 2, 2013
- R. Dangerfield, R. Wang, Hydrothermal Synthesis and Reactivity Characterization of Ceria Nanoparticles, *YSU Quest 2013*, Youngstown, Ohio USA, April 2, 2013